minerals

MDPI

Article

Inert Gas—A New Geochemical Technology for Natural Gas Hydrate Exploration in Midlatitude Permafrost

Ruiling Tang [1], Jinli Xu [1,*], Ziwan Chen [2,3], Bin Liu [1] and Jinfeng Bai [1,*]

[1] Institute of Geophysical and Geochemical Exploration, Chinese Academy of Geological Sciences, Langfang 065000, China; truiling@mail.cgs.gov.cn (R.T.); cgslbin@mail.cgs.gov.cn (B.L.)
[2] Yunnan Institute of Geological Survey, Kunming 650216, China; chenzw_cdut@outlook.com
[3] School of Earth Sciences, Chengdu University of Technology, Chengdu 610059, China
* Correspondence: xjinli@mail.cgs.gov.cn (J.X.); bjinfeng@mail.cgs.gov.cn (J.B.)

Abstract: The development of geochemical exploration technologies unaffected by marsh microorganisms is necessary to improve the prediction of wells and explore for natural gas hydrates in mid-latitude permafrost areas. Here, we examine the potential of inert gas as a new tool for the investigation of gas hydrates in permafrost areas. The study area, 150 km^2 in size, is situated in the alpine wetland landscape of the Qilian Mountains. The sampling density and depth were 2 points/km^2 and 60 cm, respectively. In total, 300 soil and headspace gas samples were collected. The chromatographic backflush technique was used to analyze the inert gases helium (He) and neon (Ne) in the headspace gas samples. A comprehensive interpretation was conducted based on geological and geochemical survey results. We propose a geogas migration mechanism of inert gases in the soil above the natural gas hydrate deposits. The inert gas anomalies near the ground surface of the Muli coalfield in the Qilian Mountains, derived from the deep hydrate deposits and fault structure, are not affected by marsh microorganisms. Thus, inert gas anomalies are practical tools for natural gas hydrate exploration in permafrost areas.

Keywords: inert gas; methane; natural gas hydrate; permafrost; geochemical exploration

Citation: Tang, R.; Xu, J.; Chen, Z.; Liu, B.; Bai, J. Inert Gas—A New Geochemical Technology for Natural Gas Hydrate Exploration in Midlatitude Permafrost. *Minerals* **2023**, *13*, 1393. https://doi.org/10.3390/min13111393

Academic Editor: Paul Alexandre

Received: 14 August 2023
Revised: 22 October 2023
Accepted: 23 October 2023
Published: 30 October 2023

1. Introduction

Natural gas hydrate (NGH) is a crystal material formed from water and light gases (mostly methane) under low-temperature and high-pressure conditions when the gas concentration is greater than its solubility [1]; it is widely distributed in submarine sediments and terrestrial permafrost regions [2–7]. The total volume of CH_4 contained in NGH deposits is very large in comparison with other global CH_4 reservoirs, and the total recoverable volume is estimated to be ~3×10^{13} m^3 [8]. Indeed, NGH has been proposed as a viable source of energy that could last throughout most of the 21st century [9]. With the increasing need for energy and stricter environmental requirements worldwide, every government attaches great importance to the development and utilization of NGH [10,11]. NGH is also the most important carbon pool in the shallow crust and is extremely sensitive to temperature and pressure changes [12–17]. The pressure and temperature requirements constrain the formation of gas hydrates in permafrost regions and marine sediments in continental margins [18,19]. Permafrost-associated gas hydrates are primarily distributed in the high-latitude permafrost regions of the Arctic [19–24]. In 2017, a production test of NGH in the Shenhu area of the South China Sea achieved stable gas production for eight consecutive days, with the cumulative gas production exceeding 120,000 cubic meters, making a historic breakthrough in the trial production of NGH [25–27]. The potential of NGH resources is significant not only in the sea but also in permafrost regions in China. Notably, between 2008 and 2009, the first gas hydrate drilling was implemented in the Qilian Mountain permafrost, and hydrate samples were obtained from wells DK-1, DK-2, DK-3, DK-7, and DK-8. However, no hydrate was found in well DK-4, located 400 m

north of the discovery wells. In 2013, a gas hydrate sample was discovered in well DK-9, located 400 m southeast of well DK-1. This significant finding represents the first discovery and detection of gas hydrate in China's permafrost, as well as in the low-middle latitude permafrost globally [7,28].

Seismic reflection and integrated geophysical well logging are still the primary exploratory technologies at present in the high-latitude permafrost regions of the Arctic [29–32]. In recent years, many geophysicists have conducted numerous studies on gas hydrates in the Qinghai–Tibet plateau permafrost [33], but nothing was found in the similar "BSR" interface. Gas hydrate location is a vast and complex engineering project. It is difficult to fulfill requirements by using only conventional seismic reflection and integrated geophysical well logging [34–36]. Thus, as in conventional oil and gas exploration [37–40], exploration geochemistry can play a decisive role as an effective complement to seismic reflection data and geophysical well logging [36,41].

Inert gases have become an effective tracer in geoscience due to their rareness and chemical inertia [42–44]. As indicated by several studies, a helium (He) anomaly in the soil is an effective tracer of deep oil and gas reservoirs [45–47]. Inert gases are trace components of natural gas hydrate deposits in sea and terrestrial areas. The He and Ne contents are 0.50–98.00 $\mu L \cdot L^{-1}$ and 1.0–7.6 $\mu L \cdot L^{-1}$, respectively [48,49]. Inert gases are typical atmophile elements, which are easily absorbed by natural gas and are common non-hydrocarbon components in natural gas [46]. NGH is very similar to conventional oil and gas in terms of source and migration mechanisms [50]. The inert gases are involved in the migration and accumulation of natural gas hydrates. It is not likely that they react chemically with other components or are affected by surface microorganisms. They easily penetrate the overlying strata and permafrost layers through microleakage and accumulate in the surface soil.

Based on geochemical research in recent years, the relationship between geochemical inert gas anomalies and natural gas hydrates and the fault structure is discussed in this paper. The vertical distribution of inert gas in drill holes and the correlation with methane are investigated. Furthermore, a formation mechanism of geochemical inert gas anomalies is proposed for natural gas hydrates.

2. Geological Setting

The study area is situated in the Juhugeng mining area of the Muli coalfield in the Qilian Mountains, which overall has a complex anticlinal structure (Figure 1). The Juhugeng mining area remains the syncline axis around 50 degrees to 70 degrees north by west, with complex anticline and syncline structures consisting of one anticline and two syncline structures [51,52]. The exposed strata in the mining area mainly include the Middle Jurassic Jiangcang Formation (J_2j) and the Muri Formation (J_2m), each containing multiple coal-bearing strata [53] serving as the key to the exploration of NGH. The Upper Triassic Galedesi Formation (T_1g), with dark mudstone, black mudstone, oil shale, and a thin coal seam as its main lithological characters, is widely exposed in the north and south of the Juhugeng mining area and at its anticlinal axis part, which stratigraphically exists in disconformity with the overlying Jurassic. This formation is the main source rock and serves as a potential oil and gas area, depending on its relatively well-developed reservoir [52].

Triassic strata occur widely in the northern and southern parts of the mining area and the anticline axis [51–53]. The lithology consists mainly of black siltstones, mudstones, and thin coal seams. The Middle Jurassic Lower Muli Group (J_2m^1) is a braided river alluvial plain deposit composed of medium–coarse-grained clastic rocks and occasionally a thin layer of carbonaceous mudstones or thin coals. The Upper Muli Group (J_2m^2) is a lake–swamp deposit composed mainly of dark-gray siltstones, fine sandstones, and gray fine- to medium-grained sandstones and coarse sandstones, among which two main coal seams are sandwiched [53]. The Middle Jurassic Lower Jiangcang Group (J_2J^1) consists mainly of gray fine-grained sandstones, medium-grained sandstones, dark-gray mudstones, and siltstones that contain two to six layers of coal. The Upper Jiangcang Group (J_2J^2) is a

thick oil shale section containing a set of fine debris mudstones and siltstones formed in shallow and semi-deep lake environments [53]. The Upper Jurassic Group (J_3) is a set of red clastic rocks formed in semi-arid and arid climates [53].

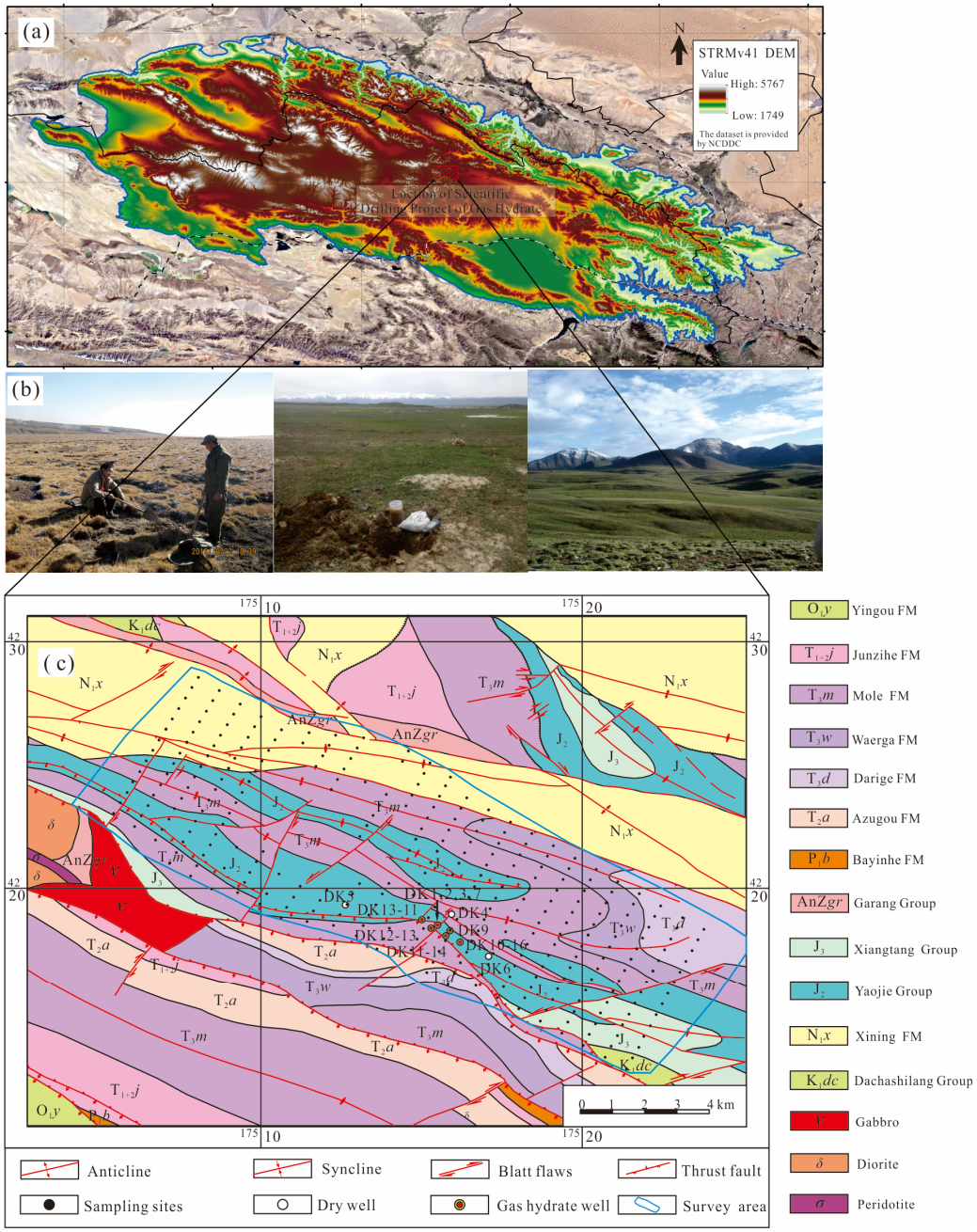

Figure 1. (**a**) Location of the Scientific Drilling Project of Gas Hydrate (The DEM dataset is provided by the National Cryosphere Desert Data Center. URL: http://www.ncdc.ac.cn/portal/metadata (accessed on 8 October 2023)). (**b**) Photos of the field investigation (Photos taken by Zhang Fugui at Muli Field Scientific Observation and Research Station). (**c**) Geological map of the study area (modified from Lu et al., 2011 [28]).

From 2008–2016, the "Scientific Drilling Project of Natural Gas Hydrate" was conducted in the Qilian Mountains by the China Geological Survey [7]. Geological, geophysical, and geochemical investigations and studies were conducted in the Qinghai–Tibet Plateau permafrost, resulting in the identification of prospective NGH-bearing areas within the region [33,36,53–57]. In 2008, NGH samples were recovered from several boreholes, and

anomalies associated with hydrates were observed in all of them [58]. Fracture-filling is the main occurrence type of NGH; it occurs as the thin-layer-like, flake, block group on the fracture surface of siltstone, mudstone, and oil shale. Pore-filling hydrate disseminated occurs in the porous sandstone and is difficult to observe with the naked eye, but it can be indirectly speculated by continuously emerging bubbles and water drops and by a dispersion-like abnormal low temperature of the infrared imaging from the core [7,58].

3. Materials and Methods

3.1. Sampling

The experimental area covered an area of 150 km^2 with a sampling density of 2 points/km^2. A total of 300 soil samples and headspace gases were collected from the study area; in addition, 400 core headspace gases were collected at DK-8. Headspace gas samples were collected using headspace bottles filled with saturated saline solution. The headspace bottles used in this study were made of high-strength polyethylene with a capacity of 500 mL (Chinese patent: CN102478463) and have high-fidelity properties [59]. The bottle cap was equipped with a silicone rubber spacer to help prevent gas escape. The purpose of filling the headspace bottles with saturated saline solution is to reduce the solubility of light hydrocarbons in aqueous solution and to force most of the light hydrocarbons to be gathered in the headspace. Soil samples of 40–60 cm were collected with a hand-held drill after removing gravel and grass roots. Each sample was placed in a bottle with 200 mL of saturated brine to increase the surface of the saturated brine to 400 mL. The bottles were tightened, placed upside down, and sent to the laboratory for analysis within three days. More details about the physically adsorbed gas sampling were described by Sun et al. [41].

3.2. Instrumental Analysis

The headspace gas samples from the cores were analyzed at the Research Institute of Petroleum Exploration and Production in Wuxi. After the samples were transported to the laboratory, the metal cans containing the samples were shaken and left to resettle for a period (generally, 24 h). A gas chromatograph (7890B, Agilent, Santa Clara, CA, USA) was used to test the gas components. The chromatographic backflush technique was used to analyze the inert gases helium (He) and neon (Ne). The chromatographic backflushing technique is a widely adopted chromatographic method, strategically employed to swiftly cleanse the chromatographic column for the efficient preparation of subsequent samples. Applied extensively in laboratories requiring high-throughput analyses, the backflushing technique enhances efficiency by minimizing cross-contamination between samples and facilitating the prompt readiness of the column for each new sample analysis [60,61]. Optimal conditions were established for gas chromatographic analysis. An analytical column packed with molecular sieve and a pre-analytical column packed with Porapak-Q were employed. High-purity nitrogen (99.999%) was used as the carrier gas. Sample injection was performed using a quantitative loop. The analysis conditions included a carrier gas flow rate of 22 mL/min, a thermal conductivity detector temperature of 150 °C, a column oven temperature of 40 °C, and a switching time of 0.78 min for the backflushing electromagnetic valve and on-change valve. The detection limit (φ) was $\leq$1.0 $L \cdot L^{-1}$. The external standard method was used for calibration. Standard samples were collected using an injection syringe under optimal analysis conditions, and standard curves were constructed. Standard gas I and standard gas II were blindly inserted and analyzed simultaneously with the samples to ensure analytical accuracy and precision. Each sample was measured 12 times, and the logarithmic difference (ΔlgC) and relative standard deviation (RSD%) between the average value and the standard value were calculated for each measured item. All SRMs met the requirement of ΔlgC < 10%, and all replicates met the requirement of RSD% < 30% in this study, ensuring the reliability of the analysis and test data.

3.3. Data Analysis

Correlation analysis was performed with SPSS 22.0 for Windows (SPSS Inc., Chicago, IL, USA). Surfer (Version 21.0, Golden Software, Co., Denver, CO, USA), and GeoIPAS (V 3.2, JW soft, Co., Urumqi, China) were used to draw the spatial distribution maps.

4. Results

4.1. Concentrations of Helium and Neon

The distribution of indexed concentrations in soils as obtained using geochemical mapping facilitates the reliable identification of hotspots with high concentration. The concentration of He in the Qilian Mountains ranges from 5.92 to 10.36 $\mu L \cdot L^{-1}$, with an average value of 7.99 $\mu L \cdot L^{-1}$, which is higher than the He concentration in the atmosphere (Table 1). The concentration of Ne ranges from 13.53 to 28.05 $\mu L \cdot L^{-1}$, with an average value of 20.8 $\mu L \cdot L^{-1}$, which is higher than that of the atmosphere (Table 1).

Table 1. Noble gas compositions of the atmosphere.

Element	Minimum	Maximum	Mean	Standard Deviation	Comments
He/$\mu L \cdot L^{-1}$	5.030	5.756	5.402	0.130	Atmosphere [62]
He/$\mu L \cdot L^{-1}$	/	/	5.240	/	Atmosphere [63]
He/$\mu L \cdot L^{-1}$	/	/	5.222 ± 0.017	/	Atmosphere [64]
Ne/$\mu L \cdot L^{-1}$	/	/	18.18	/	Atmosphere [64]
Ne/$\mu L \cdot L^{-1}$	/	/	18.2	/	Atmosphere [63]
He/$\mu L \cdot L^{-1}$	5.92	10.36	7.99	/	In this investigation
Ne/$\mu L \cdot L^{-1}$	13.53	28.05	20.8	/	

4.2. Distribution Characteristics of Helium and Neon

The cumulative frequency method was used in this paper to identify geochemical anomalies. The cumulative frequency of the first-order He anomaly was 85%–95%, corresponding to an anomaly threshold of 8.2 $\mu L \cdot L^{-1}$; the cumulative frequency of the second-order anomaly was 95%–98.5%, corresponding to an anomaly threshold of 8.4–8.6 $\mu L \cdot L^{-1}$; and the cumulative frequency of the third-order anomaly was larger than 98.5%, corresponding to an anomaly threshold > 8.6 $\mu L \cdot L^{-1}$. In total, six anomalies of He were identified in the experimental area (Figure 2), which were numbered I, II, III, IV, V, and VI, respectively. Three levels of anomalies of Ne were identified. The method used to identify these anomalies was the same as that utilized for He. The lower limit of the first-order anomaly is 21.2 $\mu L \cdot L^{-1}$, the content of the second-order anomaly ranges from 21.6 to 22.1 $\mu L \cdot L^{-1}$, and the content of the third-order anomaly is greater than 22.1 $\mu L \cdot L^{-1}$. In total, seven anomalies of He were identified in the experimental area (Figure 3), which were numbered I, II, III, IV, V, VI, and VII, respectively.

4.2.1. Distribution Characteristics of Helium

Anomaly I in the southeast of the Sanlutian coal mine is oval-shaped, moderately intense, and a second-order anomaly. It covers an area of approximately 4.25 km^2 and consists of 10 abnormal points with average and maximum values of 8.38 $\mu L \cdot L^{-1}$ and 10.2 $\mu L \cdot L^{-1}$, respectively. This anomaly extends in the NNW direction and is controlled by the regional reverse faults in the NW direction and the normal fault in the NNE direction. Earthquakes reveal that faults are the migration channels of gas hydrates [41]. Therefore, it is hypothesized that the anomalous distribution of He is influenced by the gas migration channels, which indicates a close correlation between this anomaly and deep-seated gas hydrate deposits.

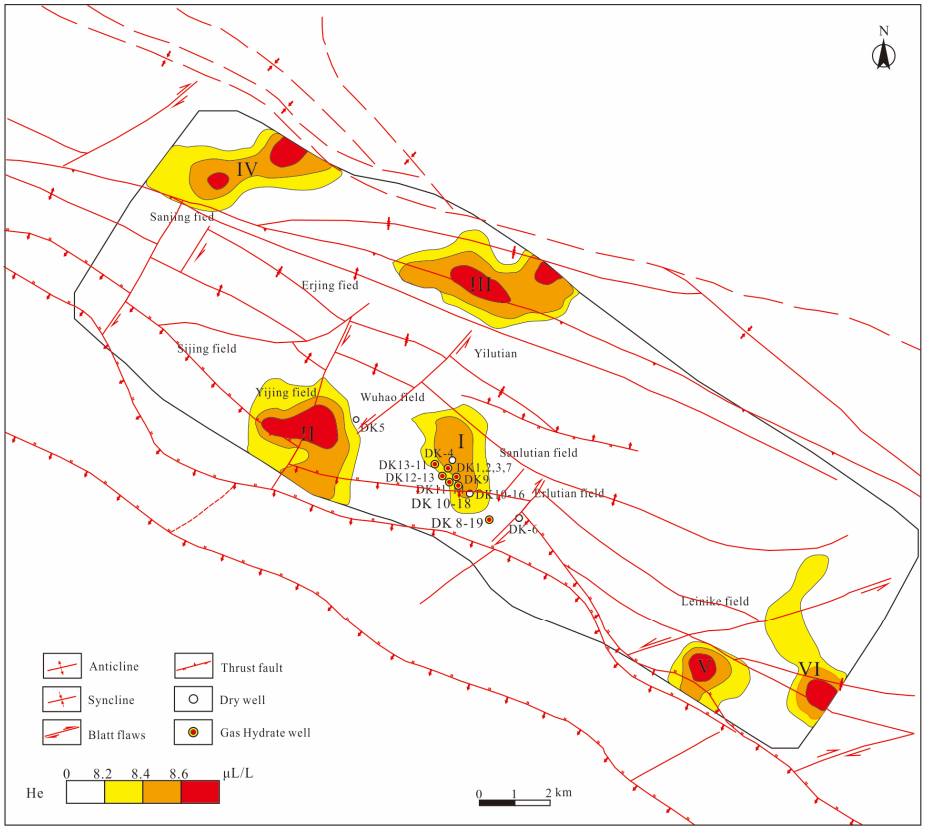

Figure 2. Geochemical anomaly and tectonic map of He in Muli in the Qilian Mountains.

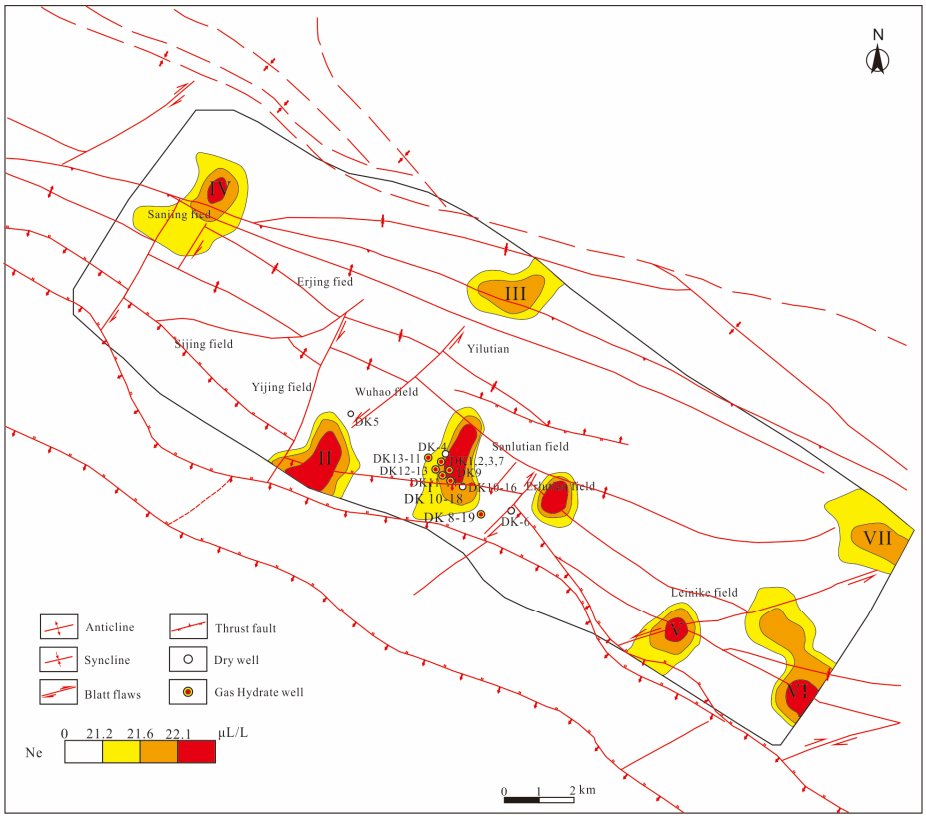

Figure 3. Geochemical anomaly and tectonic map of Ne in Muli in the Qilian Mountains.

There are nine gas hydrate wells in Sanlutian: DK-1, DK-2, DK-3, DK-7, DK-9, DK13-11, DK12-13, DK10-16, and DK11-14 (Figure 2). Four layers of gas hydrates were discovered in the DK-9 well in 2013 using geochemical exploration. Hydrate samples were collected from the four layers at depths of 188.20–209.45 m, 259.77–271.89 m, 300.09–302.19 m, and 57.50–367.59 m [65]. There are two dry wells, only one of which is located within the anomalous area (Figure 2). The success rate of He in predicting gas hydrates is 91%. Further research indicates that, in addition to the fault structure, the geological factors controlling the He anomaly also include natural gas hydrate deposits. In short, He has a relatively high success rate in predicting hydrates, which is exciting.

The distribution of Anomaly II, located in the west of Sanlutian, is controlled by the thrust faults in the southern part of the experimental area (Figure 2). The anomaly exhibits three levels of intensity. The first-order anomaly covers an area of 6.67 km^2 (mean value: 8.77 $\mu L \cdot L^{-1}$), the second-order anomaly spans 4.42 km^2 (mean value: 8.77 $\mu L \cdot L^{-1}$), and the third-order anomaly occupies 1.24 km^2 (mean value: 8.93 $\mu L \cdot L^{-1}$). Among all anomalies in the experimental area, Anomaly II is the largest and presents compelling evidence supporting its potential as a gas hydrate prospective area. There are several reasons for this assertion: (1) It exhibits a combination anomaly of He and Ne; (2) it shares similarities with the anomaly combination found in the Muli natural gas hydrate deposit, including anomalies related to the butane isomerization ratio, acidolysis hydrocarbon methane, heavy hydrocarbons, and carbonate [50]; (3) the anomaly shows a relatively strong combination of barium (Ba), iron (Fe), nickel (Ni), and calcium (Ca) [66]; and (4) the thickness of the permafrost, determined from AMT measurements, exceeds 80 m, a favorable condition for the formation of natural gas hydrate deposits [33]. Comprehensive analyses show that Anomaly II may be a natural gas hydrate anomaly associated with pyrolysis-induced gases. Well DK-5, which was drilled into the underground river channel on the edge of the anomaly, turned out to be dry. Nuclear magnetic resonance detection suggests that the significant groundwater flow in that location is unfavorable for the formation of gas hydrate deposits [33].

Anomaly III is also a combination anomaly of He and Ne. Controlled by the thrust faults in this area, the anomaly extends in the NWW direction (Figure 2). Three anomaly levels were developed. Ten first-order anomaly points cover an area of 5.50 km^2 with a mean value of 8.49 $\mu L \cdot L^{-1}$. Seven second-order anomaly points cover an area of 3.16 km^2 with a mean value of 8.77 $\mu L \cdot L^{-1}$. The third-order anomaly covers a relatively small area of less than 0.5 km^2, with a mean value of 9.55 $\mu L \cdot L^{-1}$. This anomalous area is exposed in the 158 m thick Triassic Junzihe Formation, which is primarily composed of limestone, gray–green sandstone, and siltstone. The formation is known for its high content of type II_2 organic matter that has reached a mature to highly mature stage [50]. The anomaly is characterized by an anomalous combination of acidolysis hydrocarbon methane, heavy hydrocarbons, and carbonate, which exhibit high intensities and cover a considerable abnormal area [50]. Based on the geological and geochemical analysis, it is believed that this anomaly may represent a simple hydrate prospective area.

Anomaly IV is situated in the northwest region of the experimental area (Figure 2), and no hydrate was discovered within this area. The anomaly spans an area larger than 6.58 km^2, displaying three levels of anomalies. Notably, no hydrocarbon or soil carbonate anomalies were found in this area [41,66]. It is suggested that the underlying cause of this anomaly may be attributed to a deep-seated fault structure. Anomalies V and VI, located in the southeast of the experimental area (Figure 2), exhibit combined anomalies of He and Ne. However, these anomalies do not exhibit methane, heavy hydrocarbon, or fluorescence anomalies [41,66]. Hence, it is presumed that they may be caused by regional fractures.

In summary, the anomalous distribution of He in the experimental area is primarily associated with hydrate deposits and regional faults rather than the coalfield itself.

4.2.2. Distribution Characteristics of Neon

Three levels of anomalies were observed in Anomaly I at the Sanlutian site (Figure 3), exhibiting higher intensity than the He anomaly. The first-order anomaly covers an area of 3.37 km^2, consisting of nine abnormal points and yielding a mean value of 22.68 $\mu L \cdot L^{-1}$; the second-order anomaly covers an area of 1.88 km^2, with six abnormal points and an average value of 23.29 $\mu L \cdot L^{-1}$; the third-order anomaly covers an area of approximately 1 km^2 and exhibits a mean value of 23.53 $\mu L \cdot L^{-1}$. The distribution of this anomaly is controlled by a normal fault in the NNE direction. Notably, the predictive capability of the Ne anomaly for gas hydrates aligns closely with that of He, as all gas hydrate wells are situated within the anomaly (Figure 3).

A prominent Ne anomaly, referred to as Anomaly II, was observed in the western part of the hydrate deposit, with an anomalous area of 1.44 km^2 and a mean value of 25.21 $\mu L \cdot L^{-1}$. Three levels of anomalies were observed. The anomaly covers a small but highly concentrated area (Figure 3). However, the absence of a He anomaly and a frozen soil thickness of less than 60 m [33] indicate that this anomaly is not favorable for the formation of natural gas hydrates. Geological analysis indicates that the anomaly is found to correspond to an inverted structure and is potentially associated with a deep-seated fracture of this structure.

Anomaly II of Ne corresponds to Anomaly II of He; however, its area is smaller than that of the He anomaly. Anomaly III of Ne corresponds to Anomaly III of He but has a smaller area than that of He. As mentioned above, these two anomalies might also be caused by natural gas hydrates. Anomalies IV, V, and VI of Ne correspond to Anomalies IV, V, and VI of He. Common characteristics are: (1) the lack of a hydrocarbon anomaly and (2) the anomalies being caused by regional faults.

4.3. Fractal Characteristics of He and Ne

The fractal statistical model is assumed as:

$$N(r) = Cr^{-D} \quad r > 0, \tag{1}$$

where r denotes the content of He, Ne, and CH_4; C is the proportional constant, which is >0; D is the fractal dimension, which is >0, and $N(r)$ represents the amount of He, Ne, and CH_4 in the drill core headspace gas with content equal to or greater than r.

Figure 4 shows the fractal graphs of He, Ne, and CH_4 in the drill core headspace gas at DK-8 in Sanlutian. (1) The fractal dimension of He is the largest (19.01), indicating a simple fractal. Inert gases with a simple molecular structure and small molecular radius have a strong chemical activity and can easily penetrate the overlying strata and permafrost layers to form a very strange fractal dimension. (2) Neon has a large fractal dimension of 11.52 and is also a simple fractal, indicating the relatively small data discretization and single geochemical process. (3) The fractal dimensions D_1, D_2, and D_3 of methane are 0.169, 0.847, and 0.809, respectively. Methane is multifractal and the fractal dimension is comparatively small, which indicates that various geochemical processes such as microleakage and microbial oxidation occur during the vertical migration of methane. (4) Comparison of the fractal characteristics of the inert gases and methane shows that CH_4 has a complex fractal model due to the oxidation of coalbed methane and near-surface soil microorganisms during vertical migration, while the inert gases are simple fractals because their vertical migration is not affected by the factors mentioned above.

To summarize, inert gases exhibit high penetrating power and fractal dimensions, resulting in prominent geochemical anomalies within known gas hydrate deposits as well as potential areas. The utilization of inert gases has demonstrated a remarkable success rate of up to 91% in predicting gas hydrate wells. Consequently, these gases serve as effective supplementary indicators for the exploration of gas hydrates in permafrost regions.

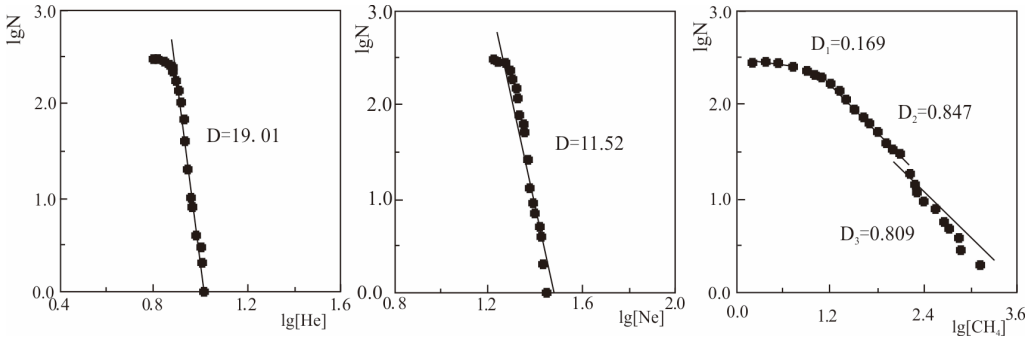

Figure 4. Fractal graphs of He, Ne, and CH_4 in the drill core headspace gas at DK-8.

5. Discussion

5.1. Vertical Distribution of Inert Gases in DK-8

To explore the migration mechanism of inert gases, the drilling debris of the gas hydrate well DK-8 in Sanlutian was collected and He, Ne, and light hydrocarbons were analyzed (Table 2).

Table 2. Inert gas content in the gas hydrate deposits in Muli and relevant characteristics.

Area	Depth/m	He/Ne	He/μL·L^{-1}	Ne/μL·L^{-1}
Atmosphere [64]		0.288	5.222 ± 0.017	18.18
Hydrate in Sanlutian	Surrounding rocks above the hydrate layer	0.40	9.70	24.4
	150–155 m of the hydrate layer	0.37	7.45	20.4
	Surrounding rocks above the hydrate layer	0.37	9.07	24.7
	227–236 m of the hydrate layer	0.36	8.12	22.5

Table 2 presents several important findings. (1) The content of He and Ne in the headspace gas of the drilling debris exceeds that of the atmosphere. (2) The surrounding rocks above the hydrate layer exhibit higher concentrations of He and Ne compared with the hydrate layer itself, which suggests the presence of distinct front halo characteristics. (3) The content of He and Ne in the hydrate layer is related to the thickness of the hydrate layer. The thicker the hydrate layer is, the higher the content of the hydrates. (4) The He/Ne ratio within the drill hole ranges from 0.36 to 0.40, surpassing the atmosphere ratio of 0.288. These anomalous geochemical characteristics of He and Ne in the surface soil, as well as their correlation with the hydrate layer within the drill hole, indicate the occurrence of differentiation and vertical microleakage of inert gases during the formation of the hydrates in the Qilian Mountains. Consequently, it becomes feasible to explore underground gas hydrate deposits by analyzing geochemical anomalies of inert gases in the near-surface soil.

5.2. Correlation between Inert Gases and Methane in the Drill Holes

The correlation between He, Ne, and CH_4 was analyzed based on the data measured on the 400 samples of core headspace gas collected at DK-8 (Figure 5). There is a strong significant correlation between He and Ne (R^2 = 0.5055) (Figure 5a), indicating that the two gases have a similar geochemical behavior during hydrate formation and microleakage. Further examination of the relationship between the inert gases and methane revealed a negative correlation between CH_4 and both He and Ne (Figure 5b,c), which implies that the vertical migration mechanism of methane is different from that of these inert gases. We hypothesize that geochemical differentiation of the hydrocarbon gases rising from the deep occurred during the formation of hydrates because the type II hydrates are unable to accommodate a significant amount of such compounds within their cage-like structure and the differentiation needs to be carried out in the hydrate stability zone. Conversely, due to their smaller molecular size, inert gases can readily penetrate the cage structure without undergoing extensive differentiation. Another important reason is that methane gas will

be oxidized by microorganisms while vertically migrating to the near-surface biochemical zone, whereas inert gases will not be affected by microbiological oxidation because of their chemical stability. The inert gases are negatively correlated with methane.

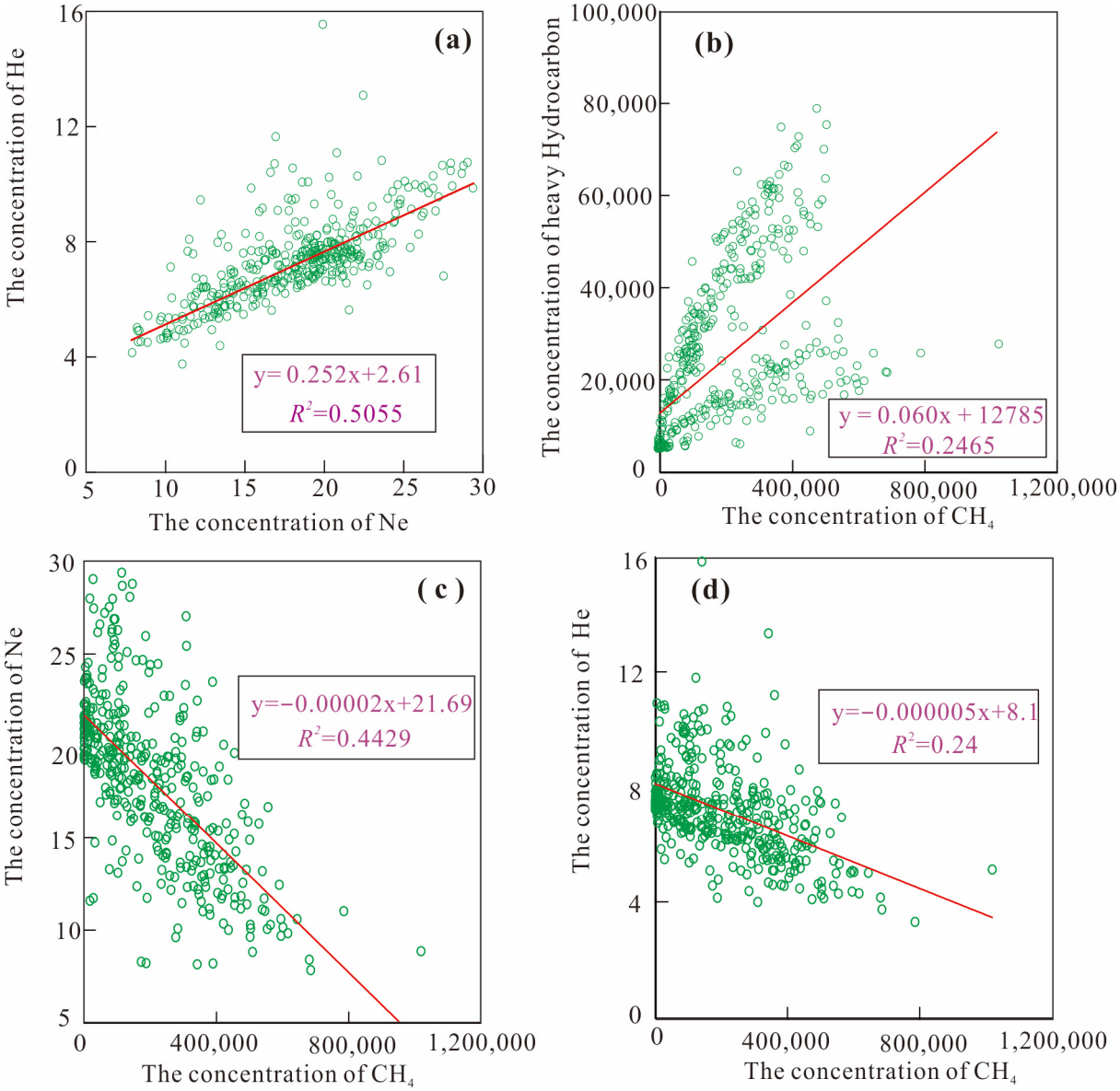

Figure 5. Correlation between inert gas concentration and hydrocarbon concentration in the headspace gas of DK-8. All units are $\mu L \cdot L^{-1}$. (**a**) Correlation between He and Ne in the headspace gas of DK-8; (**b**) Correlation between heavy hydrocarbons and CH_4 in the headspace gas of DK-8; (**c**) Correlation between Ne and CH_4 in the headspace gas of DK-8; (**d**) Correlation between He and CH_4 in the headspace gas of DK-8.

5.3. Geogas Migration Mechanism of Inert Gases

The molecular radius of inert gases is small. The molecular diameter of He is 2.28 Å and that of Ne is 2.97 Å [67]. Near-surface microorganisms do not affect inert gases because of their stable chemical properties. They take on the front halo above the hydrate deposits in permafrost areas and form a top anomaly in the soil above the hydrate deposits. Helium and neon in the drill hole are negatively correlated with methane. The formation of He and Ne anomalies is different from that of methane. Some scholars propose that the fault and fracture migration mechanisms cause the He anomaly [68–70], mainly based on the

relationship between the anomaly and the fracture system. However, it is difficult to explain the anomalies of inert gases in natural gas hydrate deposits using such a mechanism. The geogas migration mechanism of inert gases in hydrate deposits in permafrost areas is proposed in this paper. Inert gases can enter the cage structure of hydrates because of their small radius, forming the minor components of hydrate deposits in permafrost areas. The geogas current rising from the deep carries the inert gases through the overlying rocks and the permafrost layer, forming stable rocks and geochemical soil anomalies above the hydrate deposits [71,72]. The main factors controlling the geogas current migration in inert gases include the size of the hydrate deposits, the geothermal gradient, and the activity of the inert gases.

6. Conclusions

1. There are eleven gas hydrate wells in the Qilian Mountains: DK-1, DK-2, DK-3, DK-7, DK-8, DK-9, DK-12, DK13-11, DK12-13, DK11-14, and DK8-19. Ten of the eleven wells are located within the anomaly of helium and neon; only DK8-19 is situated outside the anomalous area. Experiments show that inert gases have the potential to be an effective supplementary tool for hydrate exploration in mid-latitude areas.
2. The anomalies of He and Ne are affected by neither the microorganisms in the surface marsh nor the coalbed methane. Their near-surface anomalies are in good agreement with the gas hydrates. Headspace gas technology provides a simple and convenient means of field sampling. The utilization of the same headspace gas bottle enables the concurrent analysis of light hydrocarbons and inert gas composition. This capability makes the headspace gas technology a simple technique worth popularizing in the gas hydrate exploration of permafrost areas.
3. Geogas migration refers to the microleakage of inert gases in hydrate deposits. The main factors that control the geogas migration of inert gases primarily include the size of the hydrate deposits, the geothermal gradient, and the activity of the inert gases.

Author Contributions: Conceptualization, J.X. and J.B.; methodology, R.T.; software, R.T.; formal analysis, B.L.; investigation, Z.C.; data curation, B.L.; writing—original draft preparation, R.T. and J.X.; writing—review and editing, J.B.; project administration, J.X. All authors have read and agreed to the published version of the manuscript.

Funding: This research was funded by the China Geological Survey Project, grant number DD20160224, and the Central Public Interest Scientific Institution Basal Research Fund, grant number AS2016Y01 and AS2019J02.

Data Availability Statement: The original contributions presented in the study are included in the article; further inquiries can be directed to the corresponding author.

Acknowledgments: We are grateful to Shouji Pang and Shuai Zhang from China Geological Survey and to the long-term observation base of natural gas hydrate in the Tibetan Plateau of China Geological Survey for facilitating the field work.

Conflicts of Interest: The authors declare no conflict of interest.

References

1. Sloan, E.D. Fundamental principles and applications of natural gas hydrates. *Nature* **2003**, *426*, 353–363. [CrossRef] [PubMed]
2. Kvenvolden, K.A. Gas hydrates-geological perspective and global change. *Rev. Geophys.* **1993**, *31*, 173–187. [CrossRef]
3. Kvenvolden, K.A.; Lorenson, T.D. The global occurrence of natural gas hydrate. *Am. Geophys. Union* **2001**, *124*, 3–18.
4. Collett, T.S. Permafrost–associated gas hydrate accumulations. *Ann. N. Y. Acad. Sci.* **1994**, *715*, 247–269. [CrossRef]
5. Collett, T.S.; Lee, M.W.; Agena, W.F.; Miller, J.J.; Lewis, K.A.; Zyrianova, M.V.; Boswell, R.; Inks, T.L. Permafrost–associated natural gas hydrate occurrences on the Alaska North Slope. *Mar. Pet. Geol.* **2011**, *28*, 279–294. [CrossRef]
6. Lee, S.Y.; Holder, G.D. Methane hydrates potential as a future energy source. *Fuel Process. Technol.* **2001**, *71*, 181–186. [CrossRef]
7. Zhu, Y.H.; Zhang, Y.Q.; Wen, H.J.; Lu, Z.Q.; Jia, Z.Y.; Li, Y.H.; Li, Q.H.; Liu, C.L.; Wang, P.K.; Guo, X.W. Gas hydrates in the Qilian Mountain permafrost, Qinghai, Northwest China. *Acta Geol. Sin. (Engl. Ed.)* **2010**, *84*, 1–10. [CrossRef]
8. Collett, T.S. Energy resource potential of natural gas hydrates. *AAPG Bull.* **2002**, *86*, 1971–1992.

9. Makogon, Y.F.; Holditch, S.A.; Makogon, T.Y. Natural gas-hydrates—A potential energy source for the 21st Century. *J. Pet. Sci. Eng.* **2007**, *56*, 14–31. [CrossRef]
10. Boswell, R. Is gas hydrate energy within reach? *Science* **2009**, *325*, 957–958. [CrossRef]
11. Collett, T.S.; Boswell, R.; Waite, B.W.; Kumar, P.; Roy, S.K.; Chopra, K. India national gas hydrate program expedition 02 summary of scientific results: Gas hydrate systems along the eastern continental margin of India. *Mar. Pet. Geol.* **2019**, *108*, 39–142. [CrossRef]
12. Kvenvolden, K.A. Methane hydrate in the global organic carbon cycle. *Terra Nova.* **2002**, *14*, 302–306. [CrossRef]
13. Archer, D.; Buffett, B.; Brovkin, V. Ocean methane hydrates as a slow tipping point in the global carbon cycle. *Proc. Natl. Acad. Sci. USA* **2009**, *106*, 20596–20601. [CrossRef]
14. Burton, Z.M.F.; Kroeger, K.F.; Hosford Scheirer, A.; Seol, Y.; Burgreen-Chan, B.; Graham, S. Tectonic uplift destabilizes subsea gas hydrate: A model example from Hikurangi margin, New Zealand. *Geophys. Res. Lett.* **2020**, *47*, e2020GL087150. [CrossRef]
15. Burton, Z.M.F.; Dafov, L.N. Testing the sediment organic contents required for biogenic gas hydrate formation: Insights from synthetic 3-D basin and hydrocarbon system modelling. *Fuels* **2022**, *3*, 555–562. [CrossRef]
16. Burton, Z.M.F.; Dafov, L.N. Salt Diapir-Driven Recycling of Gas Hydrate. *Geochem. Geophys. Geosystems* **2023**, *24*, e2022GC010704. [CrossRef]
17. Farahani, M.V.; Hassanpouryouzband, A.; Yang, J.H.; Tohidi, B. Insights into the climate-driven evolution of gas hydrate-bearing permafrost sediments: Implications for prediction of environmental impacts and security of energy in cold regions. *RSC Adv.* **2021**, *11*, 14334–14346. [CrossRef] [PubMed]
18. Kvenvolden, K.A. Methane hydrate—A major reservoir of carbon in the shallow geosphere? *Chem. Geol.* **1988**, *71*, 41–51. [CrossRef]
19. Collett, T.S.; Dallimore, S.R. *Permafrost-Associated Gas Hydrate//Natural Gas Hydrate*; Springer: Dordrecht, The Netherlands, 2000; pp. 43–60.
20. Wang, P.K.; Zhu, Y.H.; Lu, Z.Q.; Bai, M.G.; Huang, X.; Pang, S.J.; Liu, H.; Xiao, R. Research progress of gas hydrates in the Qilian Mountain permafrost, Qinghai, northwest China: Review. *Sci. Sin. Phys. Mech. Astron.* **2019**, *49*, 034606. [CrossRef]
21. Dallimore, S.R.; Collett, T.S. *Scientific Results from the Mallik 2002 Gas Hydrate Production Research Well Program, Mackenzie Delta, Northwest Territories, Canada*; Geological Survey of Canada: Vancouver, BC, Canada, 2005.
22. Makogon, Y.F.; Omelchenko, R.Y. Commercial gas production from Messoyakha deposit in hydrate conditions. *J. Nat. Gas Sci. Eng.* **2013**, *11*, 1–6. [CrossRef]
23. Richard, B.; Dai, J.C.; Shelander, D.; Boswell, R.; Collett, T.; Cook, A.; Dallimore, S.; Fujii, K.; Imasato, Y.; Fukuhara, M.; et al. Developments in Gas Hydrates. *Oilfield Rev.* **2010**, *22*, 18–33.
24. Lee, M.W.; Collett, T.S. In-situ gas hydrate saturation estimated from various well logs at the Mount Elbert Gas Hydrate Stratigraphic Test Well, Alaska North Slope. *Mar. Pet. Geol.* **2011**, *28*, 439–449. [CrossRef]
25. Liang, J.Q.; Zhang, W.; Lu, J.A.; Wei, J.G.; Kuang, Z.G.; He, Y.L. Geological occurrence and accumulation mechanism of natural gas hydrates in the eastern Qiongdongnan Basin of the South China Sea: Insights from site GMGS5-W9-2018. *Mar. Geol.* **2019**, *418*, 106042. [CrossRef]
26. Ye, J.L.; Qin, X.W.; Xie, W.W.; Lu, H.L.; Ma, B.J.; Qiu, H.J.; Liang, J.Q.; Lu, J.A.; Kuang, Z.G.; Lu, C.; et al. Main progress of the second gas hydrate trial production in the South China Sea. *China Geol.* **2020**, *47*, 557–568.
27. Li, J.F.; Ye, J.L.; Qin, X.W.; Qiu, H.J.; Wu, N.Y.; Lu, H.L.; Xie, W.W.; Lu, J.G.; Peng, F.; Xu, Z.Q.; et al. The first offshore natural gas hydrate production test in South China Sea. *China Geol.* **2018**, *1*, 5–16. [CrossRef]
28. Lu, Z.Q.; Zhu, Y.H.; Zhang, Y.Q.; Wen, H.J.; Li, Y.H.; Liu, C.L. Gas hydrate occurrences in the Qilian Mountain permafrost, Qinghai Province, China. *Cold Reg. Sci. Technol.* **2011**, *66*, 93–104. [CrossRef]
29. Lin, Z.Z.; Pan, H.P.; Fang, H.; Gao, W.L.; Liu, D.M. High-altitude well log evaluation of a permafrost gas hydrate reservoir in the Muli area of Qinghai, China. *Sci. Rep.* **2018**, *8*, 12596. [CrossRef] [PubMed]
30. Fang, S.; Lin, Z.; Zhang, Z.; Zhang, C.; Du, T. Gas hydrate saturation estimates in the Muli permafrost area considering bayesian discriminant functions. *J. Pet. Sci. Eng.* **2020**, *195*, 107872. [CrossRef]
31. Collett, T.S.; Johnson, A.H.; Knapp, C.C.; Bosewell, R. Natural gas hydrates: A review. *Am. Assoc. Pet. Geol. Mem.* **2009**, *89*, 146–219.
32. Boswell, R.; Moridis, G.; Reagan, M.; Reagan, M.; Collett, T.S. Gas hydrate accumulation types and their application to numerical simulation. In Proceedings of the Seventh International Conference on Gas Hydrate, Edinburgh, UK, 17–21 July 2011.
33. Fang, H.; Xu, M.C.; Lin, Z.Z.; Zhong, Q.; Bai, D.W.; Liu, J.X.; Pei, F.G.; He, M.X. Geophysical characteristics of gas hydrate in the Muli area, Qinghai province. *J. Nat. Gas Sci. Eng.* **2017**, *37*, 539–550. [CrossRef]
34. Ning, F.L.; Liang, J.Q.; Wu, N.Y.; Zhu, Y.H.; Wu, S.G.; Liu, C.L.; Wei, C.F.; Wang, D.D.; Zhang, Z.; Xu, M.; et al. Reservoir characteristics of natural gas hydrates in China. *Nat. Gas Ind.* **2020**, *8*, 1–24.
35. Lu, Z.Q.; Tang, S.Q.; Luo, X.L.; Zhai, G.Y.; Fan, D.W.; Wang, T.; Zhu, Y.H.; Xiao, R. A natural gas hydrate-oil-gas system in the Qilian Mountain permafrost area, northeast of Qinghai-Tibet Plateau. *China Geol.* **2020**, *3*, 511–523. [CrossRef]
36. Zhang, F.G.; Qin, A.H.; Zhu, Y.H.; Sun, Z.J.; Zhang, S.Y.; Wang, H.Y.; Yang, Z.B.; Zhou, Y.L. A discussion on geochemical migration mechanism of natural gas hydrate in Qilian Mountain permafrost. *Miner. Depos.* **2020**, *39*, 326–336.
37. Hunt, M.J. *Petroleum Geochemistry and Geology (A Series of Books in Geology)*; W.H. Freeman: New York, NY, USA, 1979.
38. Tissot, B.P.; Welte, D.H. *Petroleum Formation and Occurrence*; Springer: Berlin/Heidelberg, Germany, 1984.

39. Burton, Z.F.M.; Moldowan, J.M.; Sykes, R.; Graham, S.A. Unraveling petroleum degradation, maturity, and mixing and addressing impact on petroleum prospectivity: Insights from frontier exploration regions in New Zealand. *Energy Fuels* **2018**, *32*, 1287–1296. [CrossRef]
40. Burton, Z.F.M.; Moldowan, J.M.; Magoon, L.B.; Sykes, R.; Graham, S. Interpretation of source rock depositional environment and age from seep oil, east coast of New Zealand. *Int. J. Earth Sci.* **2019**, *108*, 1079–1091. [CrossRef]
41. Sun, Z.J.; Yang, Z.B.; Mei, H.; Qin, A.H.; Zhang, F.G.; Zhou, Y.L.; Zhang, S.Y.; Mei, B.W. Geochemical characteristics of the shallow soil above the Muli gas hydrate reservoir in the permafrost region of the Qilian Mountains, China. *J. Geochem. Explor.* **2014**, *139*, 160–169. [CrossRef]
42. Craig, H.; Lupton, J.E.; Primordial, N. Helium and hydrogen in oceanic basalts. *Earth Planet. Sci. Lett.* **1976**, *31*, 369–389. [CrossRef]
43. Craig, H.; Lupton, J.E. Helium isotope variations. *Trans. Am. Geophys. Union* **1978**, *59*, 1194.
44. Ciotoli, G.; Lombardi, S.; Morandi, S.; Zarlenga, F. A multidisciplinary, statistical approach to study the relationships between helium leakage and neotectonic activity in a gas province: The Vasto basin, Abruzzo-Molise (central Italy). *Am. Assoc. Pet. Geol.* **2004**, *88*, 355–372. [CrossRef]
45. Roberts, A.A. Helium manometry in exploring for hydrocarbons: Part II. In *Unconventional Methods in Exploration for Petroleum and Natural Gas II*; Southern Methodist University Press: Dallas, TX, USA, 1981.
46. Elliot, T.; Ballentine, C.J.; O'Nions, R.K.; Ricciuto, T. Carbon, helium, neon and argon isotopes in a Po basin natural gas field. *Chem. Geol.* **1993**, *106*, 429–440. [CrossRef]
47. Pinti, D.L.; Marty, B. Noble gases in crude oils from the Paris Basin, France: Implication of the origin of fluids and constraints on oil-water-gas interactions. *Geochim. Et Cosmochim. Acta* **1995**, *59*, 3389–3404. [CrossRef]
48. Ginsburg, G.D.; Soloviev, V.A.; Cranston, R.E.; Lorensen, T.D.; Kvenvolden, K.A. Gas hydrates from the continental slope, offshore Sakhalin Island, Okhotsk Sea. *Geo-Mar. Lett.* **1993**, *13*, 41–48. [CrossRef]
49. Prasolov, E.M.; Tokarev, I.V.; Ginsburg, G.D. Helium and other noble gases in gas-hydrate sediments of the Hakon Mosby Mud Volcano. *Geo-Mar. Lett.* **1999**, *19*, 84–88. [CrossRef]
50. Zhang, F.G.; Yang, Z.B.; Zhou, Y.L.; Zhang, S.; Yu, L.S. Accumulation mechanism of natural gas hydrate in the Qilian Mountain permafrost, Qinghai, China. *Front. Energy Res.* **2022**, *10*, 1006421. [CrossRef]
51. Wen, H.J.; Shao, L.Y.; Li, Y.H.; Lu, J.; Zhang, S.L. Structure and stratigraphy of the Juhugeng coal district at Muli, Tianjun County, Qinghai Province. *Geol. Bull. China* **2011**, *30*, 1823–1828.
52. Fu, J.H.; Zhou, L.F. Triassic stratigraphic provinces of the southern Qilian basin and their petro-geological features. *Northwest Geosci.* **2000**, *21*, 64–72.
53. Niu, Z.X.; Geng, Q.M.; Dou, L. Palaeogeographic analysis of Muli coalfield Juhugeng coalmine area in Qinghai Province. *Geol. Rev.* **2015**, *61*, 158–159.
54. Lu, Z.Q.; Zhu, Y.H.; Zhang, Y. Basic geological characteristics of gas hydrates in Qilian Mountain permafrost area, Qinghai Province. *Miner. Depos.* **2010**, *29*, 182–191.
55. Wang, P.K.; Huang, X.; Pang, S.J.; Zhu, Y.H.; Lu, Z.Q.; Zhang, S.; Liu, H.; Yang, K.L.; Li, B. Geochemical dynamics of the gas hydrate system in the Qilian Mountain Permafrost, Qinghai, Northwest China. *Mar. PetGeol.* **2015**, *59*, 72–90. [CrossRef]
56. Li, B.; Sun, Y.H.; Guo, W.; Shan, X.L.; Wang, P.K.; Pang, S.J.; Jia, R.; Zhang, G.B. The mechanism and verification analysis of permafrost-associated gas hydrate formation in the Qilian Mountain, Northwest China. *Mar. PetGeol.* **2017**, *86*, 787–797. [CrossRef]
57. Huang, X.; Zhu, Y.H.; Wang, P.K.; Guo, X.W. Hydrocarbon gas composition and origin of core gas from the gas hydrate reservoir in Qilian Mountain permafros. *Geol. Bull. China.* **2011**, *30*, 1851–1856.
58. Wang, P.K.; Zhu, Y.H.; Lu, Z.Q.; Huang, X.; Pang, S.J.; Zhang, S. Gas hydrate stability zone migration occurred in the Qilian mountain permafrost, Qinghai, Northwest China: Evidences from pyrite morphology and pyrite sulfur isotope. *Cold Reg. Sci. Technol.* **2014**, *98*, 8–17. [CrossRef]
59. Li, G.Z.; Hu, B. The latest progress of the analytical techniques of the petroleumgeochemical exploration in China: Problems and development direction. *Nat. Gas Geosci.* **2013**, *24*, 1171–1185.
60. Deans, D.R. An improved technique for back-flushing gas chromatographic columns. *J. Chromatogr. A* **1965**, *18*, 477–481. [CrossRef] [PubMed]
61. Li, Z.Y.; Zhou, J.L.; Zhao, J.H. Determination of He, Ne, H_2 in tank top gas by chromatographic method and its application in Helium resource survey. *Northwestern Geol.* **2022**, *55*, 267–273.
62. Ozima, M.; Podosek, F.A. *Noble Gas Geochemistry*; Cambridge Univ Press: London, UK, 1983.
63. Mamyrin, B.A.; Tolstikhin, I.N. *Helium Isotopes in Nauture*; Elsevier: Amsterdam, The Netherlands, 1984; pp. 1–173.
64. Holland, P.W.; Emerson, D.E. A determination of the helium 4 content of near-surface atmospheric air within the continental United States. *J. Geophys. Res.* **1987**, *92*, 12557–12566. [CrossRef]
65. Lu, Z.Q.; Zhu, Y.H.; Liu, H.; Zhang, Y.Q.; Jin, C.S.; Huang, X.; Wang, P.K. Gas source for gas hydrate and its significance in the Qilian Mountain permafrost, Qinghai. *Mar. Pet. Geol.* **2013**, *43*, 341–348. [CrossRef]
66. Sun, Z.J.; Yang, Z.B.; Lu, Z.Q.; Zhang, F.G.; Zhang, S.Y.; Zhou, Y.L.; Wang, H.Y. Geochemical Characteristics of Trace Elements in Soil above Sanlutian Natural Gas Hydrates in the Qilian Mountains. *Geoscience* **2015**, *29*, 1164–1172.
67. Sloan, E.D.; Koh, C.A. *Clathrate Hydrate of Natural Gases*, 3rd ed.; Taylor and Francis Group: New York, NY, USA, 2008; pp. 554–555.

68. Duddridge, G.A.; Grainger, P.; Durrance, E.M. Fault detection using soil gas geochemistry. *Quat. J. Eng. Geol.* **1991**, *24*, 427–435. [CrossRef]
69. Klusman, R.W. *Soil Gas and Related Methods for Natural Resource Exploration*; John Wiley & Sons Ltd.: Chichester, UK, 1993; p. 483.
70. Ciotoli, G.; Etiope, G.; Guerra, M.; Lombardi, S. The detection of concealed faults in the Ofanto basin using the correlation between soil-gas fracture surveys. *Tectonophysics* **1999**, *301*, 321–332.
71. Zhang, F.G.; Tang, R.L.; Zhou, Y.L.; Zhang, S.Y.; Sun, Z.J.; Wang, H.Y. A new tool for natural gas hydrate exploration in permafrost regions: Analysis of inert gas helium neon. *Acta Geol. Sin.* **2019**, *93*, 751–761.
72. Zhou, Y.L.; Sun, Z.J.; Yang, Z.B. Geochemical characteristics and implications of helium and neon in natural gas hydrates deposits in the Muli permafrost, Qilian Mountains. *Geoscience* **2018**, *32*, 995–1002.